Hybrid quantum-classical Monte Carlo study of a molecule-based magnet

P. Henelius
Theoretical Physics, Royal Institute of Technology, SE-106 91 Stockholm, Sweden

R. S. Fishman
Materials Science and Technology Division, Oak Ridge National Laboratory, Oak Ridge, Tennessee 37831-6071, USA

(Received 26 August 2008; published 5 December 2008)

Using a Monte Carlo (MC) method, we study an effective model for the Fe(II)Fe(III) bimetallic oxalates. Within a hybrid quantum-classical MC algorithm, the Heisenberg $S=2$ and $S'=5/2$ spins on the Fe(II) and Fe(III) sites are updated using a quantum MC loop while the Ising-type orbital angular momenta on the Fe(II) sites are updated using a single-spin classical MC flip. The effective field acting on the orbital angular momenta depends on the quantum state of the system. We find that the mean-field phase diagram for the model is surprisingly robust with respect to fluctuations. In particular, the region displaying two compensation points shifts and shrinks but remains finite.

DOI: 10.1103/PhysRevB.78.214405 PACS number(s): 75.50.Xx, 71.70.Ej, 75.10.Dg, 75.40.Mg

I. INTRODUCTION

Bimetallic oxalates are layered molecule-based magnets with the chemical formula $A[M(II)M'(III)(ox)_3]$.[1] Every layer contains two different transition-metal atoms, M(II) and M′(III), in the alternating honeycomb structure depicted in Fig. 1. Each bond represents an oxalate molecule ox $=C_2O_4$, which generates a crystal-field potential at both ionic sites. For different transition metals, bimetallic oxalates can be ferromagnetic, antiferromagnetic, or ferrimagnetic with moments always pointing out of the plane.[2] Since the type of magnetic order does not depend on the cation A that couples the magnetic layers, the magnetic properties of the bimetallic oxalates are primarily controlled by a single bimetallic layer.

For the Fe(II)Fe(III) bimetallic oxalates, however, the presence of magnetic compensation below the ferrimagnetic transition temperature T_c does depend on the choice of A.[3] For several cations, the magnetization in a small field is positive just below $T_c \approx 45$ K but then become negative below $T_{\rm comp} \approx 32$ K. This effect was explained by Fishman and Reboredo,[4] who used mean-field (MF) theory to solve an effective Hamiltonian that includes spin-orbit coupling on the Fe(II) sites. Magnetic compensation is produced when the orbital angular momentum $L^{\rm cf}$ of the low-lying crystal-field doublet on the Fe(II) sites exceeds a threshold value. By altering the crystal-field potential, the cation A can shift $L^{\rm cf}$ above or below this threshold value. In this paper, we use a Monte Carlo (MC) technique to study the same effective Hamiltonian and demonstrate that the MF results are surprisingly immune to the effect of fluctuations.

By Hund's first rule, the spins on the Fe(II) ($3d^6$) and Fe(III) ($3d^5$) sites are $S=2$ and $S'=5/2$, respectively. Since the Fe(III) multiplet is half full, its orbital angular momentum L' vanishes according to Hund's second rule. The $L=2$ orbital angular momentum on the Fe(II) sites is split by the C_3-symmetric crystal-field potential produced by the six oxygen atoms surrounding each ion. This splitting creates two doublets and one singlet.[4] The orbital angular momentum is unquenched when one of the doublets lies lowest in energy. In that case, the out of plane or z component of the orbital angular momentum on the Fe(II) sites takes values $\pm L^{\rm cf}$, where $L^{\rm cf}$ ranges from 0 to 2 and depends on the crystal-field potential. The spin-orbit coupling on the Fe(II) sites is given by $\lambda \mathbf{L}_i \cdot \mathbf{S}_i$, where $\mathbf{L}_i = \pm L^{\rm cf}\mathbf{z}$ and $\lambda \approx -147$ K (Ref. 5) is the spin-orbit coupling constant (negative because the $3d^6$ shell is more than half filled). The total angular momentum $\mathbf{J}_i = \mathbf{S}_i + \mathbf{L}_i$ on the Fe(II) sites is not a good quantum number and Hund's third rule is not obeyed because the crystal-field potential is large compared with the spin-orbit coupling.

Hence, the effective Hamiltonian of the Fe(II)Fe(III) bimetallic oxalates can be written as

$$H = J\sum_{\langle ij\rangle} \mathbf{S}_i \cdot \mathbf{S}'_j + \lambda \sum_i L_i^z S_i^z, \tag{1}$$

where the $\langle ij\rangle$ summation in the exchange term is performed over all nearest neighbors on the honeycomb lattice and the i summation in the spin-orbit term is performed over the Fe(II) sites only. The orbital angular momentum $L_i^z = \pm L^{\rm cf}$ can be treated as a classical variable so long as the relevant energy scales are smaller than the splitting Δ between the lowest-energy doublet and the nearest-excited states of the crystal-field potential. Since T_c is less than 45 K while Δ is larger than room temperature, this should be a good assumption for the bimetallic oxalates. For the special case where the singlet lies lowest in energy, we would take $L^{\rm cf}=0$.

Several other models can also explain the existence of magnetic compensation in the Fe(II)Fe(III) bimetallic oxalates. Nakamura[6] described the Fe(II) and Fe(III) spins by

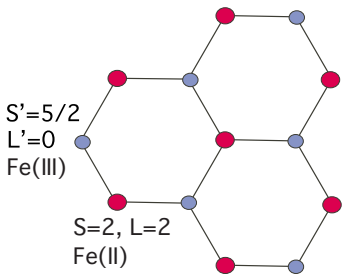

FIG. 1. (Color online) A portion of the open honeycomb lattice showing the alternating Fe(II) and Fe(III) sites.

$S=2$ and $S'=5/2$ Ising variables with single-ion anisotropy $-D(S_i^z)^2$ on the $S=2$ sites. Although magnetic compensation is found in a MF or effective-field theory treatment of this model, it is absent when the model is solved using the MC method. With fluctuations correctly included, magnetic compensation is recovered only after interlayer or longer-ranged interactions are considered. A similar conclusion was reached by Carling and Day,[7] who used MC simulations to show that next-neighbor interactions between Ising spins on the same sublattice are required to obtain magnetic compensation within a single bimetallic layer. Li *et al.*[8] treated the spins as Heisenberg operators with interlayer interactions and single-ion anisotropy on both sublattices. Using the Green's function decoupling scheme, they found that magnetic compensation occurs even in the absence of interlayer interactions when anisotropy is experienced by a single magnetic sublattice. However, it is uncertain whether magnetic compensation would survive in the presence of correlated thermal fluctuations.

Those other treatments fail to explain several important features of the Fe(II)Fe(III) bimetallic oxalates that are explained by the model Hamiltonian of Eq. (1). First, Eq. (1) provides a natural explanation for the origin of the magnetic anisotropy on the Fe(II) sites due to the splitting of the $L=2$ multiplet by the crystal-field potential. Second, unlike the model studied by Nakamura,[6] this model does not rely on interlayer interactions to produce magnetic compensation. So, it can explain the observed magnetic compensation in Fe(II)Fe(III) bimetallic oxalates with large layer separations.[3] Third, Eq. (1) explains the persistence of negative magnetization below $T_{\rm comp}$ in small fields: flipping the orbital angular momentum L_i^z requires an energy of $2|\lambda|L^{\rm cf}S \approx 175\ {\rm K} \gg T_{\rm comp}$. By contrast, the single-ion anisotropy $D \sim \lambda^2/\Delta$ experienced by the Fe(II) moments in most materials is less than 10 K.[9] Hence, the energy barrier $4D$ for flipping the Fe(II) spin is smaller than about 40 K, which is comparable to $T_{\rm comp} \approx 32$ K. Finally, Eq. (1) explains the recently observed jump[10] in the magnetization between $T_{\rm comp}$ and T_c, which is believed to arise from an inverse Jahn-Teller transition.[11] Indeed, it is difficult to explain this jump using the other models introduced above.

Magnetic compensation occurs in a MF treatment[4] of Eq. (1) for two reasons: the anisotropy at the Fe(II) sites produced by spin-orbit coupling and the Fe(II) orbital contribution to the total magnetic moment. The latter is absent in an Ising or Heisenberg ferromagnet with single-ion anisotropy. While MF theory was used to approximate the exchange coupling $J\mathbf{S}_i \cdot \mathbf{S}'_j$ between neighboring Fe(II) and Fe(III) moments, the spin-orbit coupling $\lambda \mathbf{L}_i \cdot \mathbf{S}_i$ at the Fe(II) sites was treated exactly within the crystal-field doublet. As demonstrated by Nakamura,[6] however, models that exhibit magnetic compensation within MF or effective-field theories may no longer do so once fluctuations are correctly included. So a MC study including both quantum and thermal fluctuations is needed to confirm that Eq. (1) supports magnetic compensation.

This paper is divided into four sections. In Sec. II, we describe the hybrid MC method used to study Eq. (1). The results of our MC study and a comparison with earlier MF results are presented in Sec. III. A brief conclusion is provided in Sec. IV.

II. HYBRID MC METHOD

We apply the stochastic series-expansion (SSE) quantum MC method[12] to the model Hamiltonian H. The SSE method employs a Taylor expansion of the partition function Z,

$$Z = \sum_{\alpha} \sum_{n=0}^{\infty} \frac{(-\beta)^n}{n!} \langle \alpha | H^n | \alpha \rangle, \tag{2}$$

where $|\alpha\rangle$ are the basis states used to evaluate the matrix elements of H and $\beta = 1/T$ is the inverse temperature. Quantum MC methods have been previously applied to high-spin models and here we follow the method described in Ref. 13. This section summarizes the method and emphasizes how the algorithm has been modified to treat the Ising-type orbital angular momentum. For readers interested in a detailed description of the general aspects of the SSE method, we recommend Ref. 14.

To formulate the updating procedure, we write the Hamiltonian as a sum over all nearest neighbors in the system

$$H = -J \sum_{\langle ij \rangle} H_{ij}. \tag{3}$$

The operator H_{ij} can be decomposed into its diagonal and off-diagonal parts,

$$H_{ij} = H_{D,ij} - H_{O,ij}, \tag{4}$$

where the subscript D denotes a diagonal operator and O denotes an off-diagonal operator. For the present model, these two operators take the form

$$H_{D,ij} = C - S_i^z S_j'^z + \frac{\lambda}{3J} S_i^z L_i^z \tag{5}$$

and

$$H_{O,ij} = \frac{1}{2}(S_i^+ S_j'^- + S_i^- S_j'^+). \tag{6}$$

The constant C is included in order to ensure a positive weight in the expansion.

Introducing a cutoff K in the Taylor expansion (which, when done properly, does not cause any systematic errors[14]) and including additional unit operators I, the expansion can be rewritten as

$$Z = \sum_{\alpha} \sum_{S_K} \frac{\beta^n (K-n)!}{K!} \langle \alpha | S_K | \alpha \rangle, \tag{7}$$

where S_K is the operator string

$$S_K = \prod_{p=1}^{K} H_p, \tag{8}$$

with $H_p \in \{H_{D,ij}, H_{O,ij}, I\}$. Now n is the number of bond operators $H_{D,ij}$ or $H_{O,ij}$ in the operator string S_K.[14] The MC procedure must sample the space of all states $|\alpha\rangle$ and all operator sequences S_K with the relative weight,

$$W(\alpha, S_K) = \frac{\beta^n (K-n)!}{K!} \langle \alpha | S_K | \alpha \rangle. \tag{9}$$

Denoting a propagated state by

$$|\alpha(p)\rangle = \prod_{i=1}^{p} H_i|\alpha\rangle, \tag{10}$$

the matrix element in Eq. (7) can be written as a product of elements with the form $\langle\alpha(p)|H_{ij}|\alpha(p-1)\rangle$, which is equivalent to

$$\langle S_i^z(p)L_i^z(p)S_j'^z(p)|H_{ij}|S_i^z(p-1)L_i^z(p-1)S_j'^z(p-1)\rangle.$$

We shall refer to these matrix elements as "vertices." The matrix element in Eq. (7) can be viewed as a list of such vertices.

In the operator-loop algorithm, two basic updates ensure that the complete SSE space is sampled. The diagonal update attempts to exchange diagonal operators $H_{D,ij}$ with unit operators I. The probability for inserting a diagonal operator (exchanging it for a unit operator) at position p in the operator sequence is

$$P_{\text{insert}} = \frac{N_p\beta\langle\alpha(p)|H_{D,ij}|\alpha(p)\rangle}{K-n}, \tag{11}$$

while the probability for removing a diagonal operator is

$$P_{\text{remove}} = \frac{K-n+1}{N_p\beta\langle\alpha(p)|H_{D,ij}|\alpha(p)\rangle}. \tag{12}$$

The total number of nearest-neighbor pairs on the lattice is denoted N_p. In a diagonal update, one exchange attempt is made for each diagonal and unit operator.

The second type of update is a global operator-loop update, which leaves unit operators unaffected. This update forms and flips a closed loop of spins in the vertex list. In this process, both the affected vertices and states are changed. For a detailed description of the operator-loop move, we refer to Ref. 14. In the absence of spin-orbit coupling, the operator-loop update together with the above diagonal update ensure that the complete SSE configuration space is sampled. But when spin-orbit coupling is included, the Ising-type orbital angular momentum L_i^z must also be updated. Due to the classical nature of L_i^z, no terms in the Hamiltonian are able to flip L_i^z and the orbital angular momenta must be updated in a separate move, which we describe next.

Additional flips of the spin variables S_i^z and $S_j'^z$ are allowed in case no string operator acts on sites i or j. The weight of the configuration then remains unchanged after a spin flip. The same is true for the orbital angular momenta L_i^z: if no string operator acts on a given variable L_i^z, it can be flipped with no associated change in weight.

This method must be modified at or below T_c, where many string operators act on a given L_i^z. Flipping L_i^z then causes the corresponding vertices to change with the associated weight change given by Eq. (9), which must be must be taken into account when updating the orbital angular momenta. Denoting the weight of a vertex by

$$W_p = \langle\alpha(p)|H_p|\alpha(p-1)\rangle, \tag{13}$$

then the acceptance probability of flipping an orbital momentum is

$$P = \frac{\prod_i^I W'_{p(i)}}{\prod_i^I W_{p(i)}}, \tag{14}$$

where W' indicates the weight after the flip and W indicates the weight before the flip. The product runs over all vertices containing the orbital momentum L_i^z.

The method described here works well over the range of parameters studied in this paper. It acts like a hybrid quantum-classical MC method where the Heisenberg spins are updated using a quantum MC loop algorithm but the Ising-type orbital angular momenta are updated separately using a classical single spin-flip MC method. The effective field experienced by each orbital angular momentum depends on the quantum state $\{|\alpha\rangle, S_K\}$ of the system. Since the orbital angular momenta saturate before the Heisenberg spins, it may be preferable to turn off the classical update at low temperatures in order to prevent freezing in a state different from the ground state. It is straightforward to generalize the present method to include orbital angular momenta on both magnetic sublattices,[15] which would allow the study of many other families of bimetallic oxalates. Like the standard stochastic series method, this method can also easily be generalized to arbitrary spin size.

III. TRANSITION TEMPERATURE AND PHASE DIAGRAM

We begin our discussion by considering the lattice and boundary conditions. The honeycomb lattice consists of two sites per unit cell. Using periodic boundary conditions on a two-dimensional lattice with $N\times N$ unit cells, the number of sites $N_s=2N\times N$ varies between 32 ($N=4$) and 32 768 ($N=128$). To study much larger system sizes would most likely require improvements in the algorithm.

The thermodynamic expectation value of the sublattice magnetization on the Fe(II) sites is given by

$$\langle|S^z|\rangle = \frac{2}{N_s}\left\langle\left|\sum_i S_i^z\right|\right\rangle, \tag{15}$$

where the summation runs over all $N_s/2$ sites. In a similar manner, we define the sublattice magnetization on the Fe(III) sites $\langle|S'^z|\rangle$ and the orbital angular momentum at the Fe(II) sites $\langle|L^z|\rangle$. The absolute value is measured because the strict statistical average vanishes for finite systems due to time-reversal symmetry in zero magnetic field. The total magnetization is given by

$$M = 2\langle|S'^z|\rangle - 2\langle|S^z|\rangle - \langle|L^z|\rangle, \tag{16}$$

where we take $g=2$. Recall that $\langle S^z\rangle$ and $\langle L^z\rangle$ have the same sign because λ is negative.

Sublattice magnetization curves for $\lambda=-13.3J$ and $L^{\text{cf}}=0.3$ are plotted versus temperature in Fig. 2. As shown later, these parameter values should be close to those expected for bimetallic oxalates that exhibit magnetic compensation. Many features characteristic of the general magnetization curves appear in this figure. At low temperatures, the results for different system sizes have converged to the thermody-

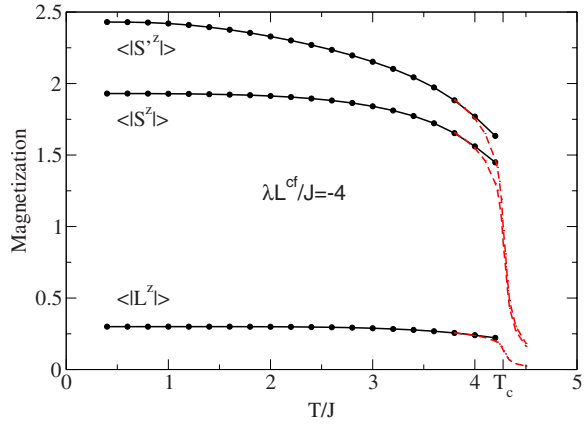

FIG. 2. (Color online) Sublattice magnetizations $\langle|S'|\rangle$, $\langle|S|\rangle$, and $\langle|L^z|\rangle$ as a function of temperature for $\lambda=-13.3J$ and $L^{cf}=0.3$. The solid and dashed lines denote results for 4×4 and 64×64 unit cells, respectively. The critical temperature is $T_c=4.28J$.

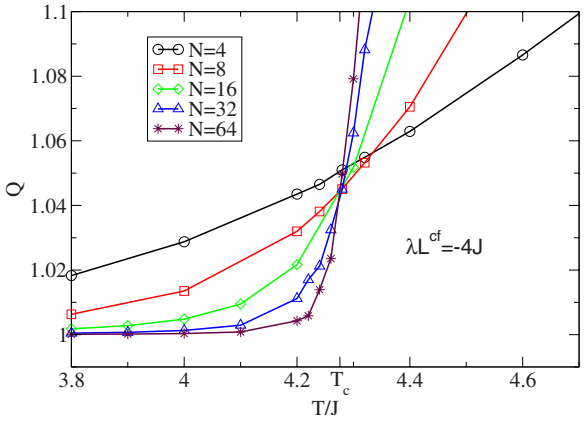

FIG. 3. (Color online) Binder ratio as a function of temperature for $\lambda L^{cf}=-4J$. Results for different system sizes intersect at the critical temperature $T_c=4.28J$. The number of sites varies from 32 ($N=4$) to 8192 ($N=64$).

namic limit. But due to the diverging correlation length, increasing finite-size effects prevent an accurate determination of the critical temperature. For the remainder of this paper, we only present those portions of the magnetization curves that have converged in system size.

At low temperatures, we can clearly see the effects of quantum fluctuations. Since the spins are treated as Heisenberg operators, the classical ground state is not an eigenstate of the Hamiltonian. The ground-state magnetizations for the $S=2$ and $S'=5/2$ sublattices are 1.91 and 2.41, respectively, or about 4% below the classical values. These deviations are small because of the relatively high-spin values. The figure also illustrates the physical mechanism responsible for magnetic compensation. Due to the effective anisotropy induced by the spin-orbit coupling to the Ising-type orbital angular momentum, the $S=2$ sublattice magnetizes faster than the $S'=5/2$ sublattice. At $T=2$ K, the S sublattice has almost reached its saturation magnetization but the S' sublattice has not.

In order to accurately determine the critical temperature, we have measured the Binder ratio[16] of the magnetization,

$$Q=\frac{\langle(S^z)^4\rangle^{1/4}}{\langle(S^z)^2\rangle^{1/2}}, \tag{17}$$

which is the ratio of two moments of the order parameter. The Binder ratio should become size independent at a second-order phase transition. After plotting the ratio for various system sizes, the point of intersection gives the critical temperature. In Fig. 3, we plot the Binder ration for $\lambda L^{cf}=-4J$, which is the value used in Fig. 2. Finite-size effects are clearly visible: the ratios for system sizes 4×4 and 8×8 intersect at $T=4.34J$ while the ratios for larger system sizes intersect at $T=4.28J$. The convergence in system size improves with increasing anisotropy.

The critical temperature depends only on the product $-\lambda L^{cf}$ and we compare the MF and MC results for T_c in Fig. 4. According to the Mermin-Wagner theorem,[17] the critical temperature of a two-dimensional system must approach zero as the anisotropy vanishes. One of the main weaknesses of the MF solution plotted in Fig. 4 is that it overestimates T_c and predicts a finite critical temperature even for an isotropic system with $-\lambda L^{cf}=0$. By contrast, the MC results in Fig. 4 indicate that T_c rises very rapidly with small $-\lambda L^{cf}$. However, even a small anisotropy induces a critical temperature of the order J. In Fig. 4, we model the rapid initial rise in the critical temperature with the functional form,

$$T_c=\frac{a}{\ln(b/|\lambda|)}. \tag{18}$$

This dependency was first reported by a renormalization-group (RG) study,[18] where the parameters a and b were related to the critical temperature of the three-dimensional isotropic model and the anisotropy parameter, respectively. Here, we simply treat a and b as fitting parameters to demonstrate that our MC results are reasonable. Notice that MF theory overestimates T_c by about 60% in almost the whole parameter range of interest. This effect must be taken into account when applying MF theory.

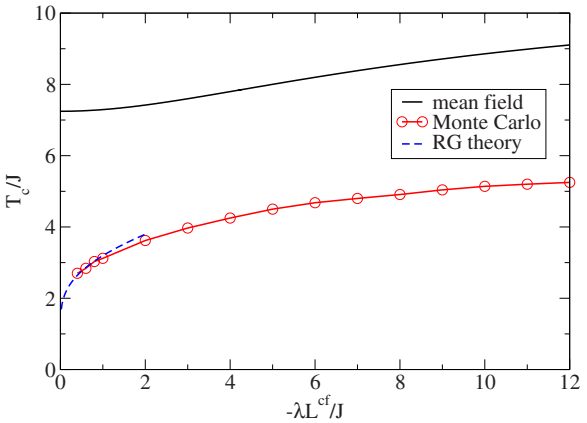

FIG. 4. (Color online) Critical temperature as a function of spin-orbit coupling $-\lambda L^{cf}$. Results from MF theory and quantum MC calculations along with the asymptotic behavior for small anisotropy from RG theory.

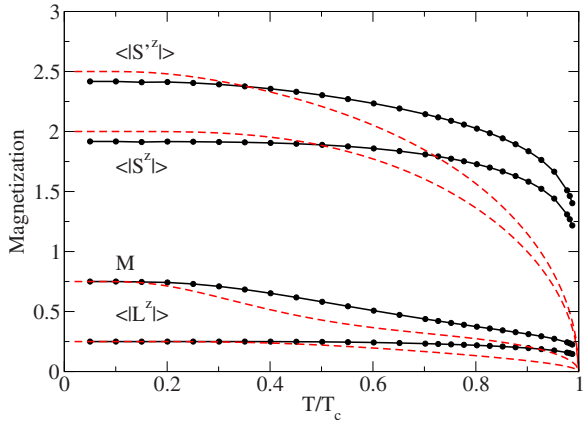

FIG. 5. (Color online) Total and sublattice magnetization calculated in MF theory (dashed line) and in the MC method (solid line) for $\lambda=-12J$ and $L^{cf}=0.25$. We display only MC data that have converged in system size, therefore not quite reaching the critical temperature.

Scaling the temperature by T_c, we compare the MC and MF results for the total and sublattice magnetizations in Fig. 5 for $\lambda=-12J$ and $L^{cf}=0.25$. Below $0.5T_c$, the classical variable L^z is essentially in its fully polarized classical ground state within both the MF and MC solutions. For the Heisenberg variables $\mathbf{S}$ and $\mathbf{S}'$, quantum fluctuations again cause deviations from the classical ground state. In the critical region, the sublattice magnetizations are described by the functional form $(T-T_c)^{\beta}$. Whereas the MF exponent is $\beta=1/2$, the Ising-type exponent $\beta=1/8$ describes the MC data. Consequently, MF theory underestimates both sublattice magnetizations as T_c is approached. The agreement between the MF and MC results for the total magnetization $M=2\langle|S'^z|\rangle-2\langle|S^z|\rangle-\langle|L^z|\rangle$ is generally better than for the individual sublattice magnetizations. Since the total spin $S^z_{tot}=\Sigma_i S^z_i+\Sigma_j S'^z_j$ commutes with H, quantum fluctuations do not effect the total magnetization at $T=0$ (Ref. 19) and $M(0)=2(S'-S)-L^{cf}$. At higher temperatures, the MF solution underestimates $M(T)$, which has the same critical exponent $\beta=1/8$ as the sublattice magnetizations.

Due to both the orbital contribution and the effects of anisotropy, the total magnetization depends sensitively on L^{cf}, as seen in Fig. 6 for $\lambda=-8J$. When L^{cf} is small, M is dominated by the $S'=2$ sublattice (defined to be positive) and it remains positive for all temperatures. When L^{cf} is large, M is dominated by the S sublattice and it remains negative for all temperatures. For intermediate values of L^{cf}, there is competition between the two sublattices. As shown, the magnetizations for $L^{cf}=0.625$ and 0.875 exhibit a compensation point T_{comp} where $M(T)$ vanishes due to a cancellation on the two sublattices.

By varying the temperature or some other control parameter such as strain,[4] the magnetization can be switched in the vicinity of a compensation point. Due to the potential applications of this effect, one main goal of this study was to determine the values of λ and L^{cf} where magnetic compensation may occur. Our main result is the phase diagram of Fig. 7 denoting the number n_{comp} of compensation points as a function of L^{cf} and λ. This phase diagram was previously

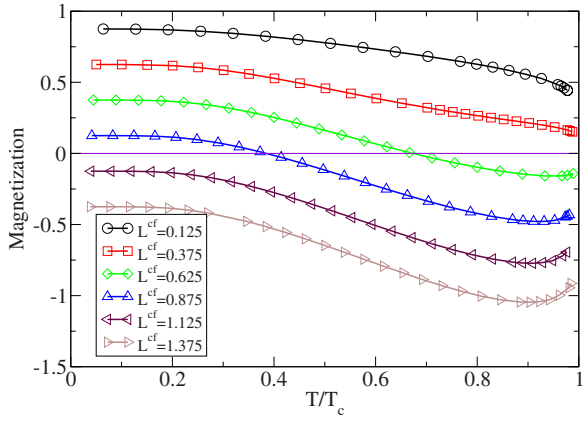

FIG. 6. (Color online) Total magnetization for $\lambda=-8J$ as a function of L^{cf} and temperature.

determined using MF theory.[4] In Fig. 7, we display the MC results on top of the MF phase diagram. Since the magnetization of the classical ground state is given by $M=1-L^{cf}$, $L^{cf}=1$ is an important dividing line: for $L^{cf}<1$, the $S'=5/2$ sublattice dominates and the ground-state magnetization is positive; for $L^{cf}>1$, the $S=2$ sublattice dominates and the ground-state magnetization is negative. When $L^{cf}<1$ and $-\lambda$ is large enough, the S sublattice may magnetize faster than the S' sublattice, producing a compensation point T_{comp} as the temperature is lowered. Similarly, when $L^{cf}>1$ and $-\lambda$ is sufficiently small, the S' sublattice may magnetize faster than the S sublattice, again causing the two sublattice magnetizations to cancel at $T_{comp}<T_c$.

The MF phase diagram contains an interesting region with not one but two compensation points. From Fig. 7, it is evident that this area has shrunk and shifted but remains finite despite the effect of fluctuations. It is impossible to say whether the MC region with $n_{comp}=2$ survives in a narrow neck for all $-\lambda/J$ greater than about 1.1. But for $-\lambda/J \geq 4.5$, there is no discernible neck of L^{cf} where two compen-

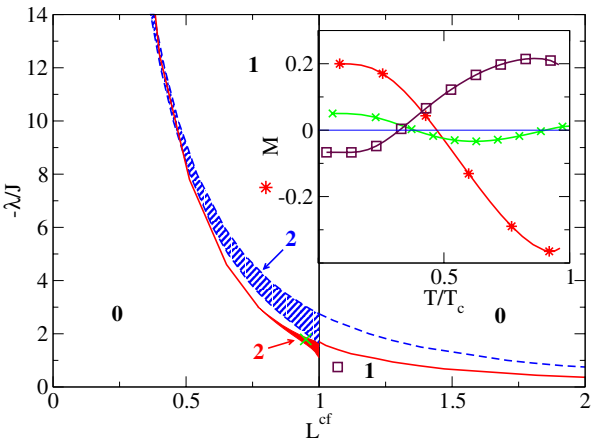

FIG. 7. (Color online) Phase diagram indicating the number of compensation points n_{comp}. The phase boundaries are given by the $L^{cf}=1$ vertical line, as well as by the dashed (MF) and solid curves (MC). Two compensation points are found in the shaded regions. In the inset are shown the MC magnetization curves for the three indicated points.

sation points can be found. So it came as a surprise when a recently studied Fe(II)Fe(III) bimetallic oxalate seemed, at first sight, to exhibit two compensation temperatures.[10] However, those measurements are more naturally explained by an inverse Jahn-Teller transition, above which the C_3 symmetry of the lattice is violated.[11]

For $L^{\mathrm{cf}}<1$, the MF curve separating the $n_{\mathrm{comp}}=2$ and 1 region lies quite close to the MC curve separating the $n_{\mathrm{comp}}=0$ and 1 region when $-\lambda/J$ is large. These two curves appear to cross at about $-\lambda/J\approx 12$. For $L^{\mathrm{cf}}>1$, the difference between the MF and MC regions with $n_{\mathrm{comp}}=1$ is much more pronounced, with the MC region about half the size of the MF region.

In the inset of Fig. 7, we show the magnetization curves for three selected points in the phase diagram. These points display either one ($L^{\mathrm{cf}}>1$ or $L^{\mathrm{cf}}<1$) or two compensation points. Notice that the $S=2$ sublattice dominates at low temperatures for the curve showing one compensation point with $L^{\mathrm{cf}}>1$.

Using the experimental results, we may now estimate the parameter values that are relevant for the Fe(II)Fe(III) bimetallic oxalates. With $\lambda=-147$ K (Ref. 5) and $T_c=45$ K, we find that $|\lambda|/T_c\approx 3.3$. The bimetallic oxalates should lie quite close to the phase boundary in Fig. 7 because some exhibit a compensation point but others do not.[3] In Fig. 2, we used the parameter values $\lambda=-13.3J$ and $L^{\mathrm{cf}}=0.3$, corresponding to $T_c=4.24J$ and $|\lambda|/T_c\approx 3.13$, which is close to the expected ratio. Since this point lies near the phase boundary in Fig. 7, it represents a reasonable estimate for the bimetallic oxalates. These estimates yield an exchange constant of $J\approx 10.6$ K, about twice the MF estimate.[4]

IV. CONCLUSION

We have studied a model for a molecule-based magnet using a hybrid quantum-classical MC method. Our main result is the phase diagram in Fig. 7, which displays the number of compensation points as a function of the spin-orbit coupling and orbital angular momentum. The region with two compensation points previously found in MF studies[4] has shrunk but remains finite.

With a simple scaling of the transition temperature, almost all MF results are qualitatively recovered in this MC study. The surprising robustness of the MF results to the effects of fluctuations arises from two factors. First, the spin values $S=2$ and $S'=5/2$ in the Fe(II)Fe(III) bimetallic oxalates are high enough that quantum fluctuations are relatively unimportant. Second, the important magnetic properties depend on the difference between the magnetic moments on the two sublattices. That difference is more immune to the effect of fluctuations than the individual sublattice moments.

Several of the discrepancies between the earlier MF results and experiments are resolved by our MC results. Within MF theory, the Curie-Weiss temperature Θ obtained from the high-temperature susceptibility $\chi\approx C/(T-\Theta)$ is always smaller in magnitude than T_c (Ref. 4) whereas experimentally it can be twice as large.[3,20] While $|\Theta|$ should remain close to its MF value even in the presence of fluctuations, T_c is reduced by about half from its MF value. Therefore, the ratio $T_c/|\Theta|$ is also suppressed by about 50% due to fluctuations.

The MC results for T_c in Fig. 4 also explain why bimetallic oxalates that exhibit magnetic compensation tend to have transition temperatures roughly 10 K higher than those that do not.[3] If materials with magnetic compensation have $-\lambda L^{\mathrm{cf}}\sim 4J$, then Fig. 4 suggests that materials without magnetic compensation will have $-\lambda L^{\mathrm{cf}}\sim 2J$ with T_c reduced by about 25%. By contrast, the MF result for T_c in Fig. 4 is relatively insensitive to $-\lambda L^{\mathrm{cf}}$ and cannot explain this sizeable suppression of the transition temperature.

Since our model Hamiltonian does not contain any interlayer couplings, T_c vanishes if the singlet lies below the doublets in the $L=2$ Fe(II) multiplet. Therefore, it seems likely that one of the doublets always lies lowest in energy even in compounds that do not exhibit magnetic compensation. Of course, neglecting the interlayer coupling was just a convenient approximation within the current treatment. While the relative insensitivity of the transition temperature to the interlayer separation and to the presence of radical spin-1/2 cations between the layers[20,21] suggests that the interlayer coupling is small, it must be present to support long-range magnetic order along the out-of-plane direction in zero magnetic field.

The present method can be easily generalized to consider spins of any size and spin-orbit coupling on both magnetic sublattices. Since quantum fluctuations grow with decreasing spin, the hybrid classical-quantum MC technique may be particularly useful when considering low-spin bimetallic oxalates such as Ni(II)Mn(III) with $S=1$ and $S'=2$. This would enable us to re-evaluate the magnetic phase diagrams obtained by Reis *et al.*,[15] where compensation was found in ranges of L and L' but quantum and thermal fluctuations were not considered. In order to improve the performance of the method, particularly close to T_c, one could use the directed-loop method[14] to minimize the backtracking process in the loop construction. Furthermore, the classical single-spin-flip update could be augmented by a cluster update.[22] We hope that the hybrid quantum-classical MC technique developed in this paper also proves of value in studies of other systems with both quantum and classical degrees of freedom.

ACKNOWLEDGMENTS

We would like to acknowledge helpful conversations with Fernando Reboredo and Anders Sandvik. P.H. acknowledges support by the Swedish Research Council. We are grateful for the generous time allocation on the Ferlin cluster managed by the Center for Parallel Computers at KTH. R.F. acknowledges support by the Laboratory Directed Research and Development Program of Oak Ridge National Laboratory managed by UT-Battelle LLC for the U. S. Department of Energy under Contract No. DE-AC05-00OR22725 and by the Division of Materials Science and Engineering of the U.S. DOE.

[1] H. Tamaki, Z. J. Zhong, N. Matsumoto, S. Kida, M. Koikawa, N. Achiwa, Y. Hashimoto, and H. Õkawa, J. Am. Chem. Soc. **114**, 6974 (1992).
[2] See the review, R. Clément, S. Decurtins, M. Gruselle, and C. Train, Monatsch. Chem. **134**, 117 (2003).
[3] C. Mathonière, S. G. Carling, and P. Day, J. Chem. Soc. Chem. Commun. **1994**, 1551; C. Mathonière, C. J. Nuttall, S. G. Carling, and P. Day, Inorg. Chem. **35**, 1201 (1996); C. J. Nuttall and P. Day, Chem. Mater. **10**, 3050 (1998).
[4] R. S. Fishman and F. A. Reboredo, Phys. Rev. Lett. **99**, 217203 (2007); Phys. Rev. B **77**, 144421 (2008).
[5] B. Bleaney and K. W. H. Stevens, Rep. Prog. Phys. **16**, 108 (1953).
[6] Y. Nakamura, J. Phys.: Condens. Matter **12**, 4067 (2000); Phys. Rev. B **62**, 11742 (2000).
[7] S. G. Carling and P. Day, Polyhedron **20**, 1525 (2001).
[8] J. Li, A. Du, and G. Wei, Physica B **348**, 79 (2004).
[9] C. Rudowicz and H. W.-F. Sung, J. Phys. Soc. Jpn. , Suppl. B **72**, 61 (2003).
[10] G. Tang, Y. He, F. Liang, S. Li, and Y. Huang, Physica B **392**, 337 (2007).
[11] R. S. Fishman, S. Okamoto, and F. A. Reboredo, Phys. Rev. Lett. **101**, 116402 (2008).
[12] A. W. Sandvik, Phys. Rev. B **59**, R14157 (1999).
[13] P. Henelius, P. Fröbrich, P. J. Kuntz, C. Timm, and P. J. Jensen, Phys. Rev. B **66**, 094407 (2002).
[14] O. F. Syljuåsen and A. W. Sandvik, Phys. Rev. E **66**, 046701 (2002).
[15] P. Reis, R. S. Fishman, F. A. Reboredo, and J. Moreno, Phys. Rev. B **77**, 174433 (2008).
[16] K. Binder, Z. Phys. B: Condens. Matter **43**, 119 (1981).
[17] N. D. Mermin and H. Wagner, Phys. Rev. Lett. **17**, 1133 (1966).
[18] M. Bander and D. L. Mills, Phys. Rev. B **38**, 12015 (1988); R. P. Erickson and D. L. Mills, *ibid.* **43**, 11527 (1991).
[19] Although we are not aware of a proof, it seems that the total $T=0$ spin for a collinear quantum ferrimagnet with sublattice spins S and $S'>S$ is given by the classical value $S'-S$. For an example with $S=1/2$ and $S'=1$, see N. B. Ivanov, J. Richter, and D. J. J. Farnell, Phys. Rev. B **66**, 014421 (2002).
[20] E. Coronado, J. R. Galán-Mascarós, C. J. Gómez-García, and J. M. Martinez-Agudo, Adv. Mater. **11**, 558 (1999); E. Coronado, J. R. Galán-Mascarós, C. J. Gómez-García, J. Ensling, and P. Gütlich, Chem. Eur. J. **6**, 552 (2000).
[21] M. Clemente-León, E. Coronado, J. R. Galán-Mascarós, and C. J. Gómez-García, Chem. Commun. (Camb.) **1997**, 1727.
[22] A. W. Sandvik, Phys. Rev. E **68**, 056701 (2003).